Purdue University

Purdue e-Pubs

International Compressor Engineering Conference

School of Mechanical Engineering

2022

Modeling, Simulation and Experimental Testing of a Two-phase Scroll Compressor

Nicolas Leclercq

Vincent Lemort

Follow this and additional works at: https://docs.lib.purdue.edu/icec

Leclercq, Nicolas and Lemort, Vincent, "Modeling, Simulation and Experimental Testing of a Two-phase Scroll Compressor" (2022). *International Compressor Engineering Conference.* Paper 2787. https://docs.lib.purdue.edu/icec/2787

This document has been made available through Purdue e-Pubs, a service of the Purdue University Libraries. Please contact epubs@purdue.edu for additional information.
Complete proceedings may be acquired in print and on CD-ROM directly from the Ray W. Herrick Laboratories at https://engineering.purdue.edu/Herrick/Events/orderlit.html

Modeling and Simulation of a Two-phase Scroll Compressor

Nicolas LECLERCQ[1*], Vincent LEMORT[1]

[1] University of Liège, Energy Systems Research Unit,
Liège, Belgium
Contact Information (+3243664823, n.leclercq@uliege.be)
* Corresponding Author

ABSTRACT

REGEN-BY-2 is a Horizon 2020 EU-funded project, that aims to develop a first-of-its-kind lab-scale prototype of a highly efficient thermodynamic cycle and related plant for the valorisation of renewable thermal energy sources, unlocking their large potential to supply electric, heating and-or cooling energy vectors. The investigated thermodynamic cycle, which will be described in the paper, is highly efficient as it is constituted by a proper combination of Carnot cycles operating with a two-phase fluid circulating in novel two-phase expanders and two-phase compressors. The aim of this paper is to present numerical investigations performed to characterize the performance of two two-phase scroll compressors being part of the plant. In this article, a compressor deterministic model is discussed, and simulations results of an off-the shelf scroll compressor are commented. No inlet tube pressure drops and no heat transfer are assumed while leakages and mechanical losses are considered in the model. For on-design operating condition (vapor quality of 39% at the compressor inlet with the HFO R1233zd(E) as a working fluid), the simulation results show a reduction of the leakages due to a sealing effect leading to volumetric efficiencies close to 100% under the given assumptions. On the contrary, isentropic efficiencies below 70% are obtained for high pressures ratios, under-compression losses being emphasized when working with two-phase flows due to high pressure drops across the discharge port.

1. INTRODUCTION

The Horizon 2020 EU-funded project REGEN-BY-2 consists in the development of a trigeneration machine allowing the simultaneous production of electric, thermal and/or cooling powers in one single system. Such CCHP (Combined Cooling, Heating and Power) targets high conversion efficiencies as it is constituted by a combination of vapor compression and expansion cycles close to the Carnot cycle, where most of the thermodynamics transformations are operated under the saturation bell of the working fluid. The working fluid selected for this application is the HFO R1233zd(E) as a results of an optimization carried out on the cycle steady-state model.

The REGEN-BY-2 cycle architecture can be found in Figure 1, furthermore, the Temperature-Entropy diagram of the design operating point is shown in Figure 2. The cycle can be divided in two main loops:

- The loop 1-2-2*-3-4-5-5*-6-7-8 consists in a two-stage vapor expansion cycle, where the high pressure is reached with the help of two compressors with a regenerator in between. Likewise, the power is recovered by three expanders, the two first being separated by the same regenerator as for the compressors. Thereby, this regenerator allows to use a part of the thermal power to increase the vapor quality in order to carry on the compression with the second compressor. The low temperature thermal source, allowing to vaporize the working fluid between point 3 and 4 can come from waste heat recovery or any renewable power source (biomass, geothermal, solar, etc). Two condensations are then performed: between point 6 and 7 in order to provide the end-user with heating and between point 8 and 1 with an air-cooled condenser.
- The second loop is realized between points 1-9-10-11-12-13. It simply consists in a refrigeration cycle in order to provide the end-user with a cooling source.

As can been seen in Figure 1, the cycle is composed of three compressors and three expanders, among these machines, four of them are working in two-phase conditions. The choice of these compression and expansion machines is of a paramount importance: these machines must handle two-phase flows while keeping high isentropic efficiencies. Considering the range of mechanical power that the machines will consume/produce on the design of the first REGEN-BY-2 prototype [1 - 2.5 kW], it appears that scroll machines are great candidates for this application due to their robustness and high isentropic efficiencies. This paper will focus on the scroll compressors designed for the REGEN-

BY-2 prototype and more specifically the ones subject to two-phase flows occurring from point 1 to 2 and point 2* to 3 on the T-s diagram presented in Figure 2.

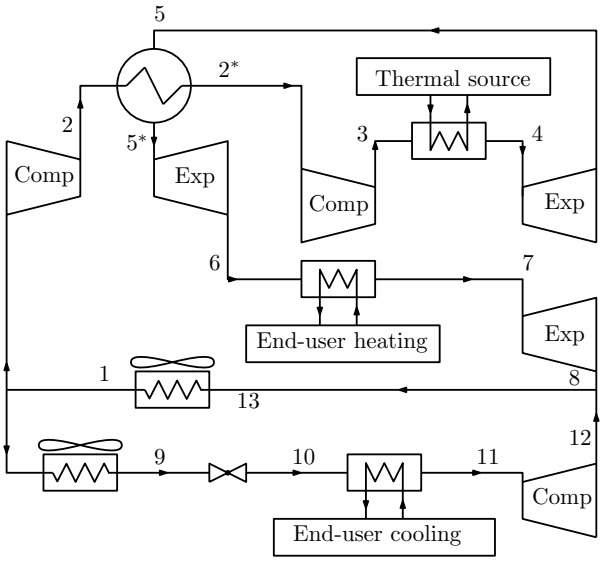

Figure 1: REGEN-BY-2 cycle architecture

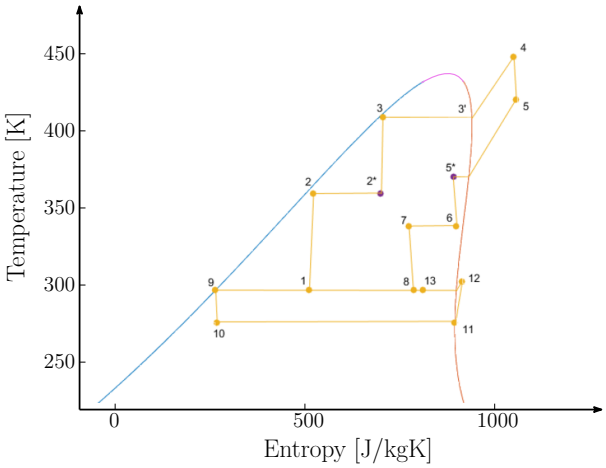

Figure 2: REGEN-BY-2 cycle Temperature-Entropy diagram

The concept of scroll compressor has been existing since the 20th century, but the first prototype of scroll compressor only appeared in the 1970's due to the small tolerances required to make the machine operating properly (Chen, Halm, Groll, & Braun, 2002). The main advantages of the scroll technology are the smooth torque variation along the compression, which generates a really low level of vibrations and makes it mechanically reliable in addition to its high efficiency and compactness (Zhao, Li, Wu, & Shu, 2005). Moreover, rotating compressors are, in general, able to handle the presence of liquid inside the compression process and, in the case of a scroll machine, could even increase the performance by lowering the leakages and the discharge temperature (Bell et al., 2012).

As there is no available off-the-shelf two-phase compressor on the market, a tailor-made design should be defined. The design of the two-phase compressors will be done with the help of a deterministic model, allowing to work with two-phase flows under really simple assumptions. The two compressions on which the machines will be designed can be found in Table 1, where the expected outlet properties have been computed assuming compressors isentropic efficiencies of 70%. From this table, one can notice that the expected inlet-outlet volume ratios are very high due to the two-phase conditions. Therefore, the expectation to get high under-compression losses are important as the built-in volume ratio of a scroll machine usually does not exceed a value of 5 (Emhardt, Tian, & Chew, 2018).

Table 1: Characteristics of the two-phase compressions.

Characteristics	Compression 1(1-2)	Compression 2 (2'-3)
Inlet temperature [K]	303	363.5
Inlet pressure [bar]	1.6	8.9
Outlet pressure [bar]	8.9	23.5
Pressure ratio [-]	5.5	2.6
Inlet vapor quality [-]	0.39	0.47
Expected outlet quality [-]	0.046	0.045
Expected volume ratio [-]	24.3	7.335
Mass flow rate [g/s]	208	208

2. SCROLL COMPRESSOR GEOMETRICAL MODEL

The development of such a geometrical model requires the knowledge of the volume and volume derivative as a function of the orbiting angle for each chamber created by the scrolls superposition. Hence, analytical forms of those volumes are needed. Indeed, numerically computing the value of the volume at each angle steps would require a huge computational time. Analytic developments for the volumes of such complex geometries have been investigated by Bell (2011). However, the need to simulate different discharge geometries than the conventional arc-arc or arc-line-arc has driven to the use of a combination between numerical calculations and analytical developments through the use of polynomial interpolations.

Thereby, by knowing the scroll involutes equations as well as the coordinates of the contact points created by the scrolls superposition, it is possible to define polygons accurately fitting the shape of the different chambers. The areas of these polygons can be computed using the following equation:

$$A = \frac{1}{2}\sum_{i=1}^{n-1} x_i y_{i+1} - x_{i+1} y_i \tag{1}$$

Where x_i and y_i are the coordinates of the n points constituting the polygon that must be closed, meaning that $(x_0, y_0) = (x_n, y_n)$. From this area, the volume can simply be obtained by multiplying it by the scroll height.

Hence, the first step of the deterministic model is to compute those areas for each chamber on an angle step of 1° for a whole rotation, 360 values will thereby be obtained for each chamber and a 5th order polynom is used to interpolate those values. Thus, the equations can be written as:

$$V = c_5\theta^5 + c_4\theta^4 + c_3\theta^3 + c_2\theta^2 + c1\theta + c_0 \tag{2}$$

$$\frac{\mathrm{d}V}{\mathrm{d}\theta} = 5c_5\theta^4 + 4c_4\theta^3 + 3c_3\theta^2 + 2c_2\theta + c1 \tag{3}$$

This technique allows, for a given geometry, to have relative errors between the volume given by the polygon area calculation and the interpolation of 0.8% for the maximum error and of 0.1% on average on a whole rotation. Nevertheless, a numerical issue can be encountered for the suction chamber for angles close to zero. Indeed, the orbiting angle is normally defined when the suction chamber starts to open, i.e. $V_s = 0$ when $\theta = 0$, however there is an absolute error that can make the volume of the chamber slightly different than zero and even negative at the beginning of the rotation, which can create too large variations and non-physical values of density and lead to convergence instabilities. A solution for this issue has been to keep the chamber volume constant for low orbiting angles ($\theta < 0.4$ rad).

The first geometry simulated with the model is taken from the retrofitting of an off-the-shelf scroll compressor that has been chosen to investigate experimentally its behavior under two-phase flows. It has a displacement volume of 80 cm^3 and a built-in volume ratio of 2.3. The representation of its geometry can be found in Figure 3 and the corresponding volume evolution in Figure 4.

3. COMPRESSOR MODEL

3.1 Assumptions

The compressor deterministic model presented in this paper relies on simple assumptions. Although the results obtained from this model give some trends of the performance sensitivity to two-phase compression, some improvements can and will be implemented to get more accurate results in the future.

The assumptions are listed as follows:

- The flow will be considered homogeneous along the compression. It means that no differentiation will be done between the two phases and the properties can be computed with a linear combination of the liquid and vapor properties. The two phases therefore have the same speed. A model like the one of (Chisholm, 1983) could be used to define 2 different phases by the mean of a parameter ψ that represents the mass fraction of liquid traveling in the gas phase at the gas velocity.

Figure 3: Compressor geometry representation

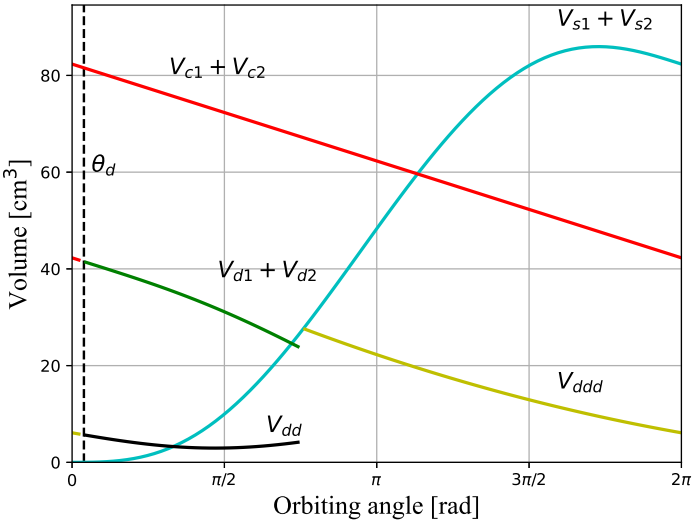

Figure 4: Volumes evolution in each chamber

- The flow will be considered in thermal equilibrium. This thermal equilibirum implies that the liquid phase and the vapor phase always have the same temperature. This assumption has also been used in Dutta, Yanagisawa, and Fukuta (2001) and Lin, Lian, and Wu (2020), although they have modeled the two phases separately using control volumes separated in two different masses and internal energies for the liquid and vapor phases, respectively. In reality, the vapor phase sees its temperature increasing during the compression while the liquid phase temperature stays first constant. Then, a heat transfer driven by the temperature difference occurs between the two phases and the vapor quality changes as well as the temperature of the two phases. The modeling of this thermal non-equilibrium has for instance been investigated by Ziviani (2017).
- Neither inlet nor outlet tubes have been modeled. Modeling those tubes would allow to get more accurate inlet and outlet conditions via the inclusion of heat transfer and pressure losses. Usually, the addition of pressure losses plays an important role to get a good estimation of the volumetric efficiency while adding heat transfer changes the outlet vapor quality of the compressor. Without the inlet pressure losses, volumetric efficiencies between 97 and 102% are obtained.
- Heat transfer model has been neither implemented between the scroll wraps and the refrigerant and nor between the scroll casing and the ambiance. Again, those models would allow to get more accuracy on the outlet quality obtained but does not change significantly the performance obtained.
- The oil circulation has not been taken into account. Adding the oil completely changes the saturation properties of the mixture, for instance, a superheated refrigerant mixed with some oil results in a part of the superheated refrigerant turning into liquid when the phase equilibrium is obtained. Besides, when an inlet vapor quality is targeted, the inlet pressure should be adapted to the oil circulation rate in order to reach this quality. These new mixture properties could be computed using, for instance, a mixing rule applied to an equation of state to figure out the fugacities of the two phases as done by França, Marcelino Neto, and Barbosa (2013), or using an activity coefficient model to compute the liquid phase fugacity and assuming an ideal gas fugacity for the vapor phase as proposed by Jia, Wang, Wang, Hu, and Sun (2020).
- Radial and flank leakages have been modeled as well as a simple mechanical model to take into account friction losses. The friction losses are assumed to leave the machine by heat transfer in the ambiance, therefore, they do not interact with the refrigerant. A part of the friction losses could have been injected in the scroll wraps and in the shell but is has not been done in this model. No check valve has been modeled meaning that under some circumstances, a backflow can occur in the discharge chamber if under-compression occurs, leading to losses of efficiency.

3.2 Overview

As a reminder, the working fluid used for the simulations is the HFO R1233zd(E), which has a normal boiling point of 19°C. The fluid properties computation is usually time consuming if the properties are directly taken from a property

library like REFPROP or CoolProp. In order to optimize the computational time of the model, it has been decided to generate properties table of R1233zd(E). Pairs of state variables like (ρ, T) are used to compute other properties like for instance the enthalpy, the internal energy or the pressure.To give an order of magnitude, using this technique allows to be 30 times faster to compute properties than by using CoolProp.

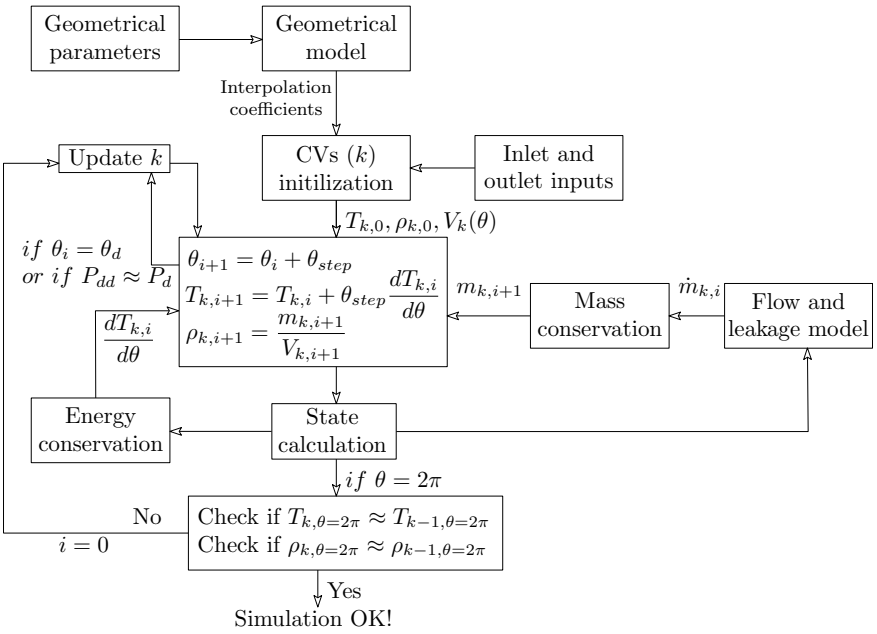

Figure 5: Structure of the deterministic model

The resolution process of the model is illustrated in Figure 5. At first, the geometrical model is run in order to get the polynomial coefficients from the volume and volume derivative curve interpolations. For each chamber, control volumes (CV) evolving along the compression have been defined. The volumes of these CVs are evolving with the orbiting angle as well as their masses via flows entering or leaving through leakages or suction/discharge processes. The application of the mass and energy conservations on these CVs allows to update the state of the CVs via the Euler forward solver. The general structure is therefore similar to what has been done in PDSim (Bell et al., 2019). The state of a CV is identified by the mean of two state variables, that allows to work in the two-phase region as well as in the superheated vapor region: the density and the temperature. The density is easily set by knowing the mass and the volume of a CV, as a reminder the two phases are assumed to be homogeneous, a mixture density can thus be defined as a function of the vapor quality Q as:

$$\rho = \left(\frac{Q}{\rho_{sat,vap}} + \frac{1-Q}{\rho_{sat,liq}} \right)^{-1} \tag{4}$$

With $\rho_{sat,vap}$ and $\rho_{sat,liq}$ the saturated density of the vapor and liquid phase, respectively.

Applying the energy conservation allows to get the derivative of the temperature with respect to the orbiting angle, as will be described in Section 3.3. At the discharge angle, the compression chambers and the discharge chamber start to merge (V_{c1} and V_{c2} become V_{d1} and V_{d2} and get connected to V_{dd}), and a mass flow rate appears between those chambers. As the discharge progresses, the pressure difference between V_{d1} and V_{d2} on one side and V_{dd} on the other side decreases. A criterion on the difference of pressure between those chambers is thereby defined: a pressure tolerance of 0.25% is necessary to consider that the chambers are merged. When a complete rotation has been performed, the state of each CV's is initialized with the final values of the previous rotation, a complete iteration has therefore been completed. At each iteration, the density and the temperature of every CV at the end of the rotation are compared with the ones of the previous iteration, if the differences are contained within a certain tolerance (0.1-0.25%), the simulation is ended up.

3.3 Mass and energy balance

As detailed in section 3.1, the energy conservation allows to get the derivative of the temperature with respect to the discharge angle while the mass conservation allows to get the updated density. Two equations are therefore used in the model: the mass conservation (Equation 5) and the energy conservation (Equation 6):

$$\frac{\mathrm{d}m_{\mathrm{cv}}}{\mathrm{d}\theta} = \frac{1}{\omega}\sum_f \dot{m}_f \tag{5}$$

$$\frac{\mathrm{d}T}{\mathrm{d}\theta} = \frac{-T\left(\frac{\partial P}{\partial T}\right)_v \left[\frac{\mathrm{d}V_{\mathrm{cv}}}{\mathrm{d}\theta} - v\frac{\mathrm{d}m_{\mathrm{cv}}}{\mathrm{d}\theta}\right] - h\frac{\mathrm{d}m_{\mathrm{cv}}}{\mathrm{d}\theta} + \frac{1}{\omega}\sum_f \dot{m}_f h_f}{m_{\mathrm{cv}}\left(\frac{\partial u}{\partial T}\right)_v} \tag{6}$$

Where the index 'f' states for 'flow path', and accounts for the flows entering of leaving the control volume while ω is the speed of the compressor [rad/s]. As can be noticed in Equation 6, the term $\left({}^{\partial u}/_{\partial T}\right)_v$ is not assumed as being the constant volume heat capacity (c_v) of the fluid, indeed, this term has to take into account the latent heat energy of the phase change, and is thus computed with a numerical derivative under this form. Regarding the term ${}^{\partial P}/_{\partial T}$, it does not need to be calculated for a constant volume as being computed in the two-phase region, it is calculated with the Clapeyron equation:

$$\left(\frac{\partial P}{\partial T}\right)_v = \frac{\partial P}{\partial T} = \frac{h_g - h_l}{T(v_g - v_l)} \tag{7}$$

3.4 Mechanical model

As already mentioned, the friction work is assumed to be equal to the ambient losses, thereby, they do not interact with the refrigerant but only contribute to deteriorate the compressor efficiency. The mechanical power consumption of the machine can be defined as:

$$\dot{W}_{cons} = \dot{W}_i + \dot{W}_{loss} = \dot{m}(h_{dis} - h_{su}) + \omega(\tau_0 + \omega\tau_1) \tag{8}$$

With τ_0 and τ_1, parameters defining the friction torque that have to be calibrated.

3.5 Flow model

The flows along primary flow paths (i.e. the suction, the discharge and the merging between the discharge chambers) are similar to the flow in a convergent nozzle and are thus considered adiabatic, reversible and compressible. For two-phase adiabatic compressible flow in a nozzle, the following expression is used for calculating the mass flow rate (Chisholm, 1983):

$$\dot{m} = \xi X_{dis} C_{dis} A_{th} \sqrt{\frac{2\int_{P_{down}}^{P_{up}} v_e \, dP}{v_{e,down}^2 - \sigma v_{e,up}^2}} \tag{9}$$

Where *xi* is the friction flow correction factor introduced by (Bell, 2011), X_d is the area correction factor, C_d is the discharge coefficient (C_d = 0.77), A_{th} is the throat area of the nozzle (i.e. the flow area of the flow path) and σ is the area ratio of downstream to upstream areas. In the developed model, X_d is considered equal to unity but this value can be calibrated with experimental data, while σ is taken equal to zero. The effective volume v_e is defined as:

$$v_e = \left[Qv_g + K_e(1-Q)v_l\right]\left[Q + \frac{1-Q}{K_e}\right] \tag{10}$$

With the effective slip ratio K_e that represents the ratio between the vapor phase and liquid phases speeds, defined as:

$$K_e = \left[\psi + \frac{(1-\psi^2)}{K-\psi}\right] \tag{11}$$

With the entrainment slip ratio given by:

$$K = \psi + (1-\psi)\sqrt{\frac{1+\psi(1-Q)v_l/(Qv_g)}{1+\psi(1-Q)/Q}}\sqrt{\frac{v_g}{v_l}} \tag{12}$$

Where ψ is the mass fraction of liquid that travels in the gas phase at the gas velocity (usually under the shape of droplets). Having $\psi = 0$ means that we have completely separated flow and the speeds are independent ($K_e = 0$) while when $\psi = 1$ the flow is homogeneous and is thus traveling at one single speed. The two-phase flow in this model has been modeled as being homogeneous which means that a value of 1 has been used for ψ. This model has been used to model the suction and discharge flows, however, it cannot be used for the leakages, as the friction has to be considered due to shape of the flow areas. Bell (2011) introduced a correction factor to adapt the mass flow rate given by Chisholm, these correlations have been implemented in the proposed model (see Equation 9), this correction factor *xi* is equal to one for flows that are not related to leakages.

Eventually, choked mass flow rates have also been investigated, using a critical pressure ratio calculated with a two-phase isentropic expansion coefficient k^* introduced by Petrovic and Stevanovic (2016).

4. SENSITIVITY ANALYSIS

The efficiency used to characterize the machine performance is an isentropic efficiency defined as:

$$\eta_{is} = \frac{\dot{m}(h_{dis,is} - h_{su})}{\dot{W}_{cons}} \tag{13}$$

Where h_{dis} is the discharge enthalpy, and $\dot{W}_{cons}$, the mechanical power consumption of the compressor.

4.1 Investigation on the compression nominal point

In this sub-section, the evolution of the different chambers' characteristics will be analysed for the compressor presented in Section 2 and the conditions of the first compression presented in Table 1, with a compressor speed of 3100 RPM. At first, the pressure and the quality of each chamber will be analyzed, their graphs can respectively be found in Figure 6 and Figure 7.

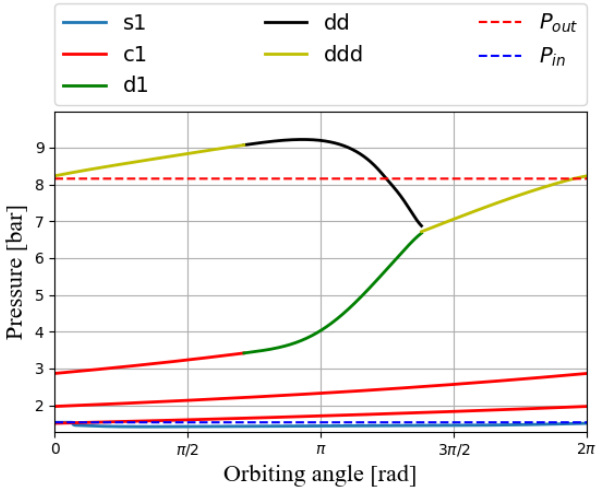

Figure 6: Pressure as a function of the orbiting angle in each chamber

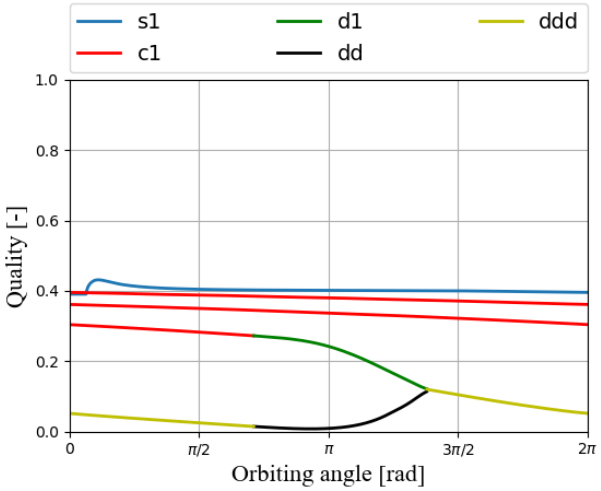

Figure 7: Quality as a function of the orbiting angle in each chamber

After a complete rotation in the s1 chamber, the compression starts and the pressure reaches approximately 2.8 bar before the discharge process starts. At this point, it is already clear that an under-compression occurs. The merging between the chamber dd and d1 and d2 then starts and finishes after more or less a third of rotation. At the end of the merging process, the pressure is far below the outlet pressure, meaning that a backflow is occuring, as no check valve has been modeled. The discharge process then continues and a complete cycle has been performed. Regarding the vapor quality, one can see that a full liquid-state is almost reached in chamber dd. It is due to the high pressure losses encountered through the discharge port that rises the pressure inside the discharge chamber. For this specific point, the isentropic efficiency obtained is 57.5% while the volumetric efficiency reaches 102%, indeed, as observed in Figure 17, the pressure of chamber s1 at the end of the rotation is higher than the inlet pressure, this is due to the reduction of suction volume at the end of the rotation and also to the inlet tube that are not modeled. This phenomenon has already been experienced by Nieter (1988). Finally, the mass flow rate is 92 g/s and the power consumption 1.31 kW.

4.2 Influence of the speed

The speed of the compressor also has an influence on its efficiency, this is true with and without leakages inside the compressor. In Figure 8, the variation of efficiency with respect to the compressor speed is plotted for two different compression ratios, with and without leakages.

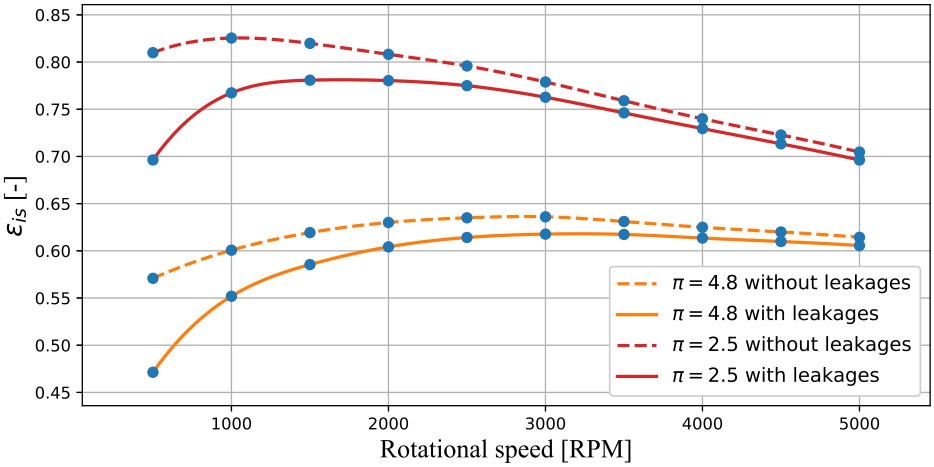

Figure 8: Variation of the isentropic efficiency with respect to the rotational speed for different pressure ratios with and without leakages

The low efficiency at low speeds is due to the greater effect of the under-compression, the pressure equilibrium between chambers d1, d2 and dd is so slowly reached that more mass has time to enter the discharge chamber from the discharge port, leading to a higher compression work as can be seen when comparing the P-V diagrams in Figure 9 and Figure 10. For higher speeds, the pressure losses are increasing due to the higher mass flow rates, thus lowering the efficiency. For a pressure ratio of 2.5, which is close to a perfect compression, the highest efficiencies can be found at the lowest speeds, because the under-compression effect does not occur in this case. In general, the leakages tend to decrease the efficiency, however, this effect is greater for low speeds, as the residence time of the fluid in the compressor is higher, it is experiencing more leakages. Therefore, the effect of the leakages is reduced for higher speeds.

4.3 Influence of the pressure ratio and inlet quality

The efficiency obtained with a vapor quality of 0.39 and a 10 K superheated vapor can be seen in Figure 11. The maxima in efficiency correspond to a perfect compression while lower pressure ratios correspond to an over-compression and higher pressure ratios to an under-compression. It can clearly be seen that the maximum is not necessarily at the same compression ratio for the two inlet qualities tested, this is due to the inlet-outlet volume ratios that are different. Indeed, the perfect compression corresponds to a pressure ratio for which the inlet/outlet volume ratio is equal to the built-in volume ratio of the machine. However, for a given inlet/outlet volume ratio, the corresponding pressure ratio is higher for a superheated vapor than for a low quality vapor. Furthermore, the under-compression losses are less important for a superheated vapor, as less pressure losses are encountered during the backflow, leading to less irreversibilities. One last observation that can be done is the impact of the quality on the leakages, it is clear that a lower quality acts as a

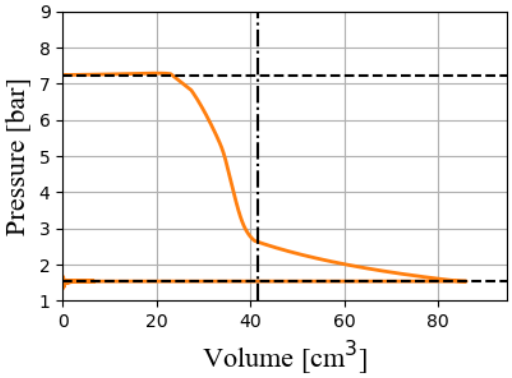

Figure 9: P-V diagram of a pressure ratio of 4.8 and a rotational speed of 500 RPM without leakages

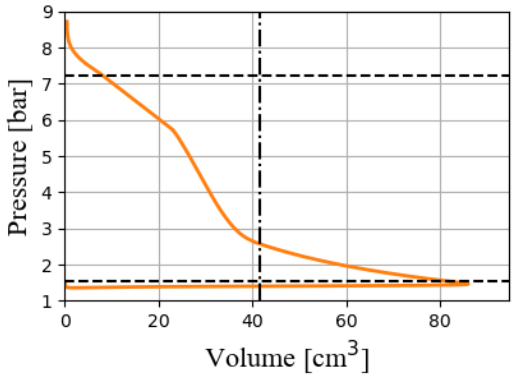

Figure 10: P-V diagram of a pressure ratio of 4.8 and a rotational speed of 5000 RPM without leakages

sealing effect for the leakages, which makes the drop of efficiency relatively lower.

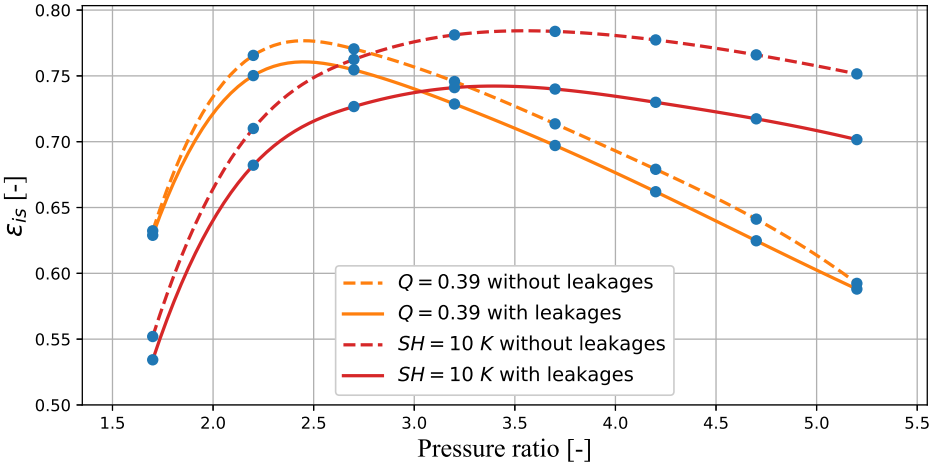

Figure 11: Variation of the isentropic efficiency with respect to the pressure ratio for different inlet qualities with and without leakages

5. CONCLUSIONS

The complete development of a deterministic model able to simulate scroll compressors working with two-phase flows has been presented. Although this model has been developed using simple assumptions like homogeneous flow, phase equilibrium and no heat transfer model, it is able to give some predictions on how this two-phase flows affect the performance of the machine. This model helped to understand how a two-phase flow machines that will be placed on the REGEN-BY-2 prototype should be designed. The results have shown that, when working with two-phase flows, for a given pressure ratio, the built-in volume ratio should be higher than the one used to work with superheated vapor. Moreover, working with two-phase flows significantly increases the pressure losses, and therefore the irreversibilities, the good design of the discharge port is thus of a paramount importance. Moreover, for the points that have to be tested, it is clear that the selected machine is not adapted due to its really low built-in volume ratio. An optimal speed of the compressor has been found, the leakages being lower with a low quality, a lower speed can be afforded allowing to reduce the pressure losses without degrading the efficiency.

Finally, as can be understood, some improvements can still be implemented in this model, even though it was already accurate enough to give a rough idea of the behavior of the compressor under two-phase flows. However, experimental data is necessary to calibrate and validate the model before confirming or updating the results presented in this paper. The authors think that the general trends will be confirmed.

NOMENCLATURE

A	Area	(m^2)	π	pressure ratio	(-)
(x,y)	coordinates	(m)	σ	area ratio	(-)
V	Volume	(m^3)	ψ	mass fraction	(-)
v	specific volume	(m^3/kg)	K	slip ratio	(-)
T	temperature	(K)	**Subscript**		
P	pressure	(bar)	cv	control volume	
h	enthalpy	(J/kg)	sat	saturation	
u	internal energy	(J/kg)	g	gas	
Q	vapor quality	(-)	l	liquid	
m	Mass	(kg)	e	effective	
$\dot{m}$	Mass flow rate	(kg/s)	f	flowpath	
ρ	density	(kg/m^3)	i	indicated	
ω	rotation speed	(rad/s)	dis	discharge	
θ	orbiting angle	(rad)	su	supply	
ε	efficiency	(-)	cons	consumed	
SH	superheat	(K)	s	isentropic	

REFERENCES

Bell. (2011). Theoretical and experimental analysis of liquid flooded compression in scroll compressors, PhD thesis at Purdue University.

Bell, Lemort, V., Groll, E. A., Braun, J. E., King, G. B., & Horton, W. T. (2012). Liquid-flooded compression and expansion in scroll machines – part I: Model development. *International Journal of Refrigeration*, *35*(7), 1878-1889.

Bell, Ziviani, D., Lemort, V., Bradshaw, C., Mathison, M., Horton, W., … Groll, E. (2019, 11). Pdsim: A general quasi-steady modeling approach for positive displacement compressors and expanders.

Chen, Y., Halm, N. P., Groll, E. A., & Braun, J. E. (2002). Mathematical modeling of scroll compressors—part I: compression process modeling. *International Journal of Refrigeration*, *25*(6), 731-750.

Chisholm, D. (1983). *Two-phase flow in pipelines and heat exchangers*. G. Godwin. Retrieved from `https://books.google.be/books?id=4qGwAAAAIAAJ`

Dutta, A. K., Yanagisawa, T., & Fukuta, M. (2001). An investigation of the performance of a scroll compressor under liquid refrigerant injection. *International Journal of Refrigeration*, *24*(6), 577-587.

Emhardt, S., Tian, G., & Chew, J. (2018). A review of scroll expander geometries and their performance. *Applied Thermal Engineering*, *141*, 1020-1034.

França, R., Marcelino Neto, M., & Barbosa, J. (2013, 01). Phase equilibrium data and thermodynamic modeling of the system r-1234yf and polyol ester lubricant oil..

Jia, X., Wang, J., Wang, X., Hu, Y., & Sun, Y. (2020). Phase equilibrium of r1234yf and r1234ze(e) with poe lubricant and thermodynamic performance on the evaporator. *Fluid Phase Equilibria*, *514*, 112562.

Lin, J., Lian, Y., & Wu, J. (2020, 04). Numerical investigation on vapor-liquid two-phase compression in the cylinder of rotary compressors. *Applied Thermal Engineering*, *170*, 115022.

Nieter, J. J. (1988). Dynamics of scroll suction process. *International Compressor Engineering Conference, Purdue University*.

Petrovic, M., & Stevanovic, V. (2016, 01). Two-component two-phase critical flow. *FME Transaction*, *44*, 109-114.

Zhao, Y., Li, L., Wu, H., & Shu, P. (2005). Theoretical and experimental studies of water injection scroll compressor in automotive fuel cell systems. *Energy Conversion and Management*, *46*(9), 1379-1392.

Ziviani, D. (2017). Theoretical and experimental characterization of single-screw expanders for orc applications, PhD thesis at Ghent University.

ACKNOWLEDGMENT

The project source of the results presented in this paper has received funding from the European Union's Horizon 2020 research and innovation programme under grant agreement N° 851541.